Growth, catalysis, and faceting of α-Ga$_2$O$_3$ and α-(In$_x$Ga$_{1−x}$)$_2$O$_3$ on m-plane α-Al$_2$O$_3$ by molecular beam epitaxy (EP)

View Online   Export Citation   CrossMark

Martin S. Williams,[1,a] (iD) Manuel Alonso-Orts,[1,2,b] (iD) Marco Schowalter,[1] (iD) Alexander Karg,[1] (iD) Sushma Raghuvansy,[1] (iD) Jon P. McCandless,[3] (iD) Debdeep Jena,[3,4,5] (iD) Andreas Rosenauer[1,2] (iD) Martin Eickhoff,[1,2] (iD) and Patrick Vogt[1,c] (iD)

AFFILIATIONS

[1] Institute of Solid State Physics, University of Bremen, Otto-Hahn-Allee 1, 28359 Bremen, Germany
[2] MAPEX Center for Materials and Processes, University of Bremen, Bibliothekstraße 1, 28359 Bremen, Germany
[3] School of Electrical and Computer Engineering, Cornell University, 229 Phillip's Hall, 14853 New York, USA
[4] Department of Material Science and Engineering, Cornell University, Bard Hall, 14853 New York, USA
[5] Kavli Institute at Cornell for Nanoscale Science, Cornell University, Ithaca, New York 14853, USA

[a] Electronic mail: marwilli@uni-bremen.de
[b] Electronic mail: alonsoor@uni-bremen.de
[c] Author to whom correspondence should be addressed: pvogt@uni-bremen.de

ABSTRACT

The growth of α-Ga$_2$O$_3$ and α-(In$_x$Ga$_{1−x}$)$_2$O$_3$ on m-plane α-Al$_2$O$_3$(10$\bar{1}$0) by molecular beam epitaxy (MBE) and metal-oxide-catalyzed epitaxy (MOCATAXY) is investigated. By systematically exploring the parameter space accessed by MBE and MOCATAXY, phase-pure α-Ga$_2$O$_3$(10$\bar{1}$0) and α-(In$_x$Ga$_{1−x}$)$_2$O$_3$(10$\bar{1}$0) thin films are realized. The presence of In on the α-Ga$_2$O$_3$ growth surface remarkably expands its growth window far into the metal-rich flux regime and to higher growth temperatures. With increasing O-to-Ga flux ratio (R_O), In incorporates into α-(In$_x$Ga$_{1−x}$)$_2$O$_3$ up to $x \leq 0.08$. Upon a critical thickness, β-(In$_x$Ga$_{1−x}$)$_2$O$_3$ nucleates and, subsequently, heteroepitaxially grows on top of α-(In$_x$Ga$_{1−x}$)$_2$O$_3$ facets. Metal-rich MOCATAXY growth conditions, where α-Ga$_2$O$_3$ would not conventionally stabilize, lead to single-crystalline α-Ga$_2$O$_3$ with negligible In incorporation and improved surface morphology. Higher T_{TC} further results in single-crystalline α-Ga$_2$O$_3$ with well-defined terraces and step edges at their surfaces. For $R_O \leq 0.53$, In acts as a surfactant on the α-Ga$_2$O$_3$ growth surface by favoring step edges, while for $R_O \geq 0.8$, In incorporates and leads to a-plane α-(In$_x$Ga$_{1−x}$)$_2$O$_3$ faceting and the subsequent ($\bar{2}$01) β-(In$_x$Ga$_{1−x}$)$_2$O$_3$ growth on top. Thin film analysis by scanning transmission electron microscopy reveals highly crystalline α-Ga$_2$O$_3$ layers and interfaces. We provide a phase diagram to guide the MBE and MOCATAXY growth of single-crystalline α-Ga$_2$O$_3$ on α-Al$_2$O$_3$(10$\bar{1}$0).

I. INTRODUCTION

The ultra-wide bandgap semiconductor gallium oxide (Ga$_2$O$_3$) has experienced tremendous interest in high-power electronics, whose development is essential to reduce energy loss in power converters.[1] Monoclinic (β-) Ga$_2$O$_3$ can be easily n-type doped by Sn, Si, or Ge. The availability of commercial β-Ga$_2$O$_3$ substrates reduces the material costs for device production compared to other wide bandgap materials, such as SiC or GaN.[2]

Other polymorphs of Ga$_2$O$_3$, such as the orthorhombic structure (ε/κ-Ga$_2$O$_3$) or the corundum structure (α-Ga$_2$O$_3$), can also be epitaxially grown, with the latter being the polymorph with the widest bandgap, of $E_g \approx 5.3$ eV,[3] and isostructural to α-Al$_2$O$_3$. This allows bandgap engineering of α-(Al$_x$Ga$_{1−x}$)$_2$O$_3$ on α-Al$_2$O$_3$ over the whole composition range of $0 \leq x \leq 1$[3] as the phase-stability of α-(Al$_x$Ga$_{1−x}$)$_2$O$_3$ on α-Al$_2$O$_3$ increases with increasing Al content.[4] The growth of high-quality β-(Al$_x$Ga$_{1−x}$)$_2$O$_3$ thin films and the fabrication of high-electron-mobility transistors based on

21 March 2024 19:46:19

β-$(Al_xGa_{1-x})_2O_3$ are limited to $x \lesssim 0.3$.[5,6] Those features of α-Ga_2O_3 provide an alternative route to develop high Al-mole fraction $(Al_xGa_{1-x})_2O_3$ alloys for high power electronics.

The epitaxial growth of α-Ga_2O_3 and α-$(Al_xGa_{1-x})_2O_3$ on α-Al_2O_3 has been investigated by molecular beam epitaxy (MBE),[3,4,7,8] chemical vapor deposition (CVD),[9,10] and pulsed laser deposition (PLD).[11,12] In conventional MBE (hereafter named "MBE"), i.e., by using elemental Ga and active O as source materials, the growth of Ga_2O_3 is limited by the formation and subsequent desorption of its volatile suboxide Ga_2O and complex two-step kinetics.[13] This growth kinetics hampers the adsorption-controlled growth of Ga_2O_3 in the Ga-rich regime, where its growth ceases in the excess of Ga adsorbates;[14,15] thus, Ga_2O_3 is typically grown in the O-rich regime.

These growth features have a detrimental impact on the crystalline and transport properties of Ga_2O_3 thin films; for example, Ga vacancies (V_{Ga}) formed in β-Ga_2O_3 when grown in the O-rich regime may act as compensating acceptors.[16] To suppress the formation of V_{Ga} and, thus, potentially improve the electrical properties of α-Ga_2O_3, its growth in the Ga-rich regime with improved crystalline quality is desirable.[8,17]

To overcome the detrimental growth kinetics of Ga_2O_3 occurring during MBE growth, a new MBE variant has been recently developed: metal-oxide-catalyzed epitaxy (MOCATAXY).[18] This growth method is based on metal-exchange catalysis (MEXCAT)[19,20] and the use of the catalysts In, Sn, In_2O, or SnO.[21] MOCATAXY expands the growth window of β-Ga_2O_3, β-$(Al_xGa_{1-x})_2O_3$, α-Ga_2O_3, ε/κ-Ga_2O_3, and In_2O_3 deep into the metal-rich regimes and enables higher T_{TC} while generally improving the properties, such as crystalline quality and surface roughness, of the thin films.[8,18,19,21–24] MOCATAXY, with In as a catalyst, emerges due to the favorable formation of intermediate and higher reaction efficiencies of In_2O_3 over Ga_2O_3 and the subsequent thermodynamically driven exchange of In–O bonds by Ga–O bonds[19] and is mathematically explained for elemental and molecular catalysts in Ref. 21.

To stabilize α-Ga_2O_3 on α-Al_2O_3 by MBE, the crystalline orientation of the α-Al_2O_3 substrate is crucial. For example, when growing α-$Ga_2O_3(0001)$/α-$Al_2O_3(0001)$ after just 3–4 monolayers of pseudomorphically grown α-$(Al_xGa_{1-x})_2O_3(0001)$, a phase transformation into β-Ga_2O_3 occurs, presumably due to strain relaxation of α-$(Al_xGa_{1-x})_2O_3$ above a film thickness (d) of $d > 2$ nm.[25–27] The growth of α-$Ga_2O_3(01\bar{1}2)$ on r-plane α-$Al_2O_3(01\bar{1}2)$ results in c-plane facets forming from $d \approx 5$ nm, which induces the nucleation and growth of β-Ga_2O_3 on top of α-$Al_2O_3(01\bar{1}2)$ at $d \approx 217$ nm.[7] Phase-pure $Ga_2O_3(11\bar{2}0)$ on a-plane α-$Al_2O_3(11\bar{2}0)$ by MBE has been limited to $d \approx 14$ nm.[26] The growth of α-Ga_2O_3 on m-plane α-$Al_2O_3(10\bar{1}0)$ was demonstrated by MBE[3,4] and MOCATAXY.[8] MBE works report stable α-Ga_2O_3 growth.[3,4] Very recently, the growth of phase-pure α-Ga_2O_3 on α-$Al_2O_3(10\bar{1}0)$ by MOCATAXY using In as the catalyst was shown to result in improved crystalline properties for α-Ga_2O_3 films, with $(10\bar{1}1)$ facets formed on top of α-$Ga_2O_3(10\bar{1}0)$.[8]

Following Ref. 8, in this work we provide a comprehensive study of the kinetic and thermodynamic growth features of α-Ga_2O_3 and α-$(In_xGa_{1-x})_2O_3$ synthesized by MBE and MOCATAXY. The purpose of this work is to systematically investigate the growth parameter space accessible by MBE and MOCATAXY on the kinetic and thermodynamic growth processes that lead to α-Ga_2O_3 and α-$(In_xGa_{1-x})_2O_3$ formation. As a first approach, we study α-Ga_2O_3 films of $d \approx 50$ nm formed on α-$Al_2O_3(10\bar{1}0)$. We find that both the oxygen-to-gallium flux ratio (R_O) and the indium-to-gallium flux ratio (R_{In}) determine the phase formation, the cation composition in α-$(In, Ga)_2O_3$, and the surface features of the thin films grown. Single-crystalline α-$Ga_2O_3(10\bar{1}0)$ is achieved in metal-rich conditions and the presence of In, with step edges formed at the surface for higher growth temperatures (T_{TC}) of 825 °C. We develop a growth and phase diagram for the growth of phase-pure α-Ga_2O_3 and α-$(In_xGa_{1-x})_2O_3$ by MBE and MOCATAXY.

II. EXPERIMENTAL

α-Ga_2O_3 thin films were grown by MBE and MOCATAXY in a Riber Compact 12 system equipped with an Oxford Applied Research HD25rf plasma source. Ga and In metals (6N purity) were supplied from standard effusion cells. The α-$Al_2O_3(10\bar{1}0)$ substrates were backside sputter-coated with a $Ti_{0.1}W_{0.9}$ alloy of thickness $d \approx 500$ nm to enable radiative substrate heating during growth. All substrates were cleaned with deionized water and rinsed with isopropanol (IPA) to remove contamination from the dicing process, followed by an ultrasonic bath in acetone for one minute, followed by an IPA rinse, and dried by N_2. To eliminate residual surface contamination, a 10-min plasma cleaning at 800 °C with O flux $\phi_O = 0.75$ standard cubic centimeters per minute (SCCM) and radio-frequency plasma-power $P_{rf} = 300$ W was carried out *in situ*.

The growth temperature is defined as T_{TC}, which was set by a thermocouple located a small distance from the substrate heater. Due to the geometry of the setup, we expect the actual growth temperature, i.e. the temperature at the surface of the substrate, to be lower than that value. Temperature variations between different growth days due to heater power variations were compensated by using an optical pyrometer operating at a wavelength of 980 nm. Reflection high-energy electron diffraction (RHEED) was used for *in situ* growth monitoring, and a retractable ion gauge was located at the growth position to measure the Ga flux (ϕ_{Ga}) and In flux (ϕ_{In}) as beam equivalent pressure (BEP) in mbar. The O flux was supplied in SCCM, and active O (ϕ_O) was generated by the radio frequency plasma source. To convert the measured BEP into physical units and to allow for the reproducibility of our results in other MBE systems, we convert ϕ_{Ga} and ϕ_{In} as mbar → nm min^{-1} → nm^{-2} s^{-1} and ϕ_O as SCCM → nm min^{-1} → nm^{-2} s^{-1} (at a given $P_{rf} = 300$ W) using the procedure established in Ref. 28. To achieve this, Ga_2O_3 and In_2O_3 calibration films were grown under conditions where all supplied cations and anions are incorporated into the respective thin film, i.e., when the sticking coefficients of Ga, In, and O are equal. This is normally the case in the O-rich regime and with $T_{TC} < 500$ °C.[29] The density of the desired atoms in the unit cell is determined by crystallographic software (here VESTA[30]). The particle fluxes of ϕ_{Ga}, ϕ_{In}, and ϕ_O can be explicitly calculated as

$$\phi_i = C \times \Gamma \times \rho_i \qquad (1)$$

with the growth rate (Γ) in nm min^{-1}, atomic density (ρ_i) of species $i = $ Ga, In, O, and conversion factor $C = 1/60$ to convert min → sec. The maximum available active ϕ_O for Ga → Ga_2O_3 and In → In_2O_3 oxidation can then be extracted from the Γ-peak at given T_{TC}, i.e.,

TABLE I. Summary of values for ϕ_{Ga}, ϕ_{In}, ϕ_O, and T_{TC} for samples grown by MBE and MOCATAXY. For the MBE and MOCATAXY grown samples, the conversions from mbar $\rightarrow$ nm^{-2} s^{-1} are ϕ_{Ga} = 5.2×10^{-7} mbar $\cong$ 4 nm^{-2} s^{-1}, ϕ_{In} = 1.2×10^{-7} mbar $\cong$ 0.44 nm^{-2} s^{-1}, ϕ_O = 0.25 SCCM $\cong$ 1.6 nm^{-2} s^{-1} (P_{rf} = 300 W). The active ϕ_O in In-mediated catalysis is multiplied by 2.8.[8,19] The growth time was adjusted to control the layer thickness.

Growth parameters	Conventional MBE	MOCATAXY
ϕ_{Ga} (nm^{-2} s^{-1})	4.0	4.0
ϕ_{In} (nm^{-2} s^{-1})	0	0.4–3.2
ϕ_O (SCCM)	0.25–0.75	0.25–0.75
Active ϕ_O (nm^{-2} s^{-1})	1.6–4.8	4.5–13.4
T_{TC} (°C)	775	775

TABLE II. Overview of samples studied in this work by MBE (R_{In} = 0) and MOCATAXY (R_{In} > 0), with $R_{In} = \phi_{In}/\phi_{Ga}$, $R_O = \phi_O/\phi_{Ga}$, and constant ϕ_{Ga} = 4.0 nm^{-2} s^{-1}. Samples A12, D2, and B12 are intermediate samples and provide additional granularity to the results provided by primary samples where necessary.

	R_O = 0.40	R_O = 0.53	R_O = 0.80	R_O = 1.20
R_{In} = 0.79	$\cdots$	$\cdots$	B4	$\cdots$
R_{In} = 0.34	A3	$\cdots$	B3	C3
R_{In} = 0.11	A2	D2	B2	C2
R_{In} = 0.05	A12	$\cdots$	B12	$\cdots$
R_{In} = 0	A1	$\cdots$	B1	C1

Γ at stoichiometric growth conditions for Ga$_2$O$_3$ and In$_2$O$_3$.[28] A summary of the calculated fluxes, as well as R_O and R_{In}, is given in Tables I and II.

High-resolution x-ray diffraction (HRXRD) and x-ray reflectometry were performed with a Philips X'Pert Pro-MRD using Cu K$_{\alpha 1}$ radiation to identify film thickness, crystal phase, and determine the composition of α-(In$_x$Ga$_{1-x}$)$_2$O$_3$. Surface morphologies were measured, and root-mean squared (rms) roughnesses were determined by atomic force microscopy (AFM) in a Bruker Dimension Icon XR scanning probe microscope. An FEI Nova 200 focused ion beam was utilized to prepare selected samples for cross-sectional structural and chemical analysis. Scanning transmission electron microscopy (STEM) in high-angle annular dark-field imaging (HAADF) mode, using a probe-corrected Thermo Fisher Scientific Spectra 300 operating at an acceleration voltage of 300 kV, was employed to measure the atomic structure of the thin films, formed facets, and interfaces. Spatially resolved energy-dispersive x-ray spectroscopy (EDX) was performed with the Super-X detection system to measure the Al, Ga, and In concentrations. Micro-Raman (μ-Raman) spectroscopy was performed for further phase identification and analysis using a Kimmon HeCd laser with a wavelength of 442 nm and a LabRAM HR Evolution confocal spectrometer.

III. RESULTS AND DISCUSSION

A. Growth kinetics by MBE and MOCATAXY

In Fig. 1(a), Γ as a function of R_{In} at a different R_O at T_{TC} = 775 °C is plotted. See Table II for the growth parameters of

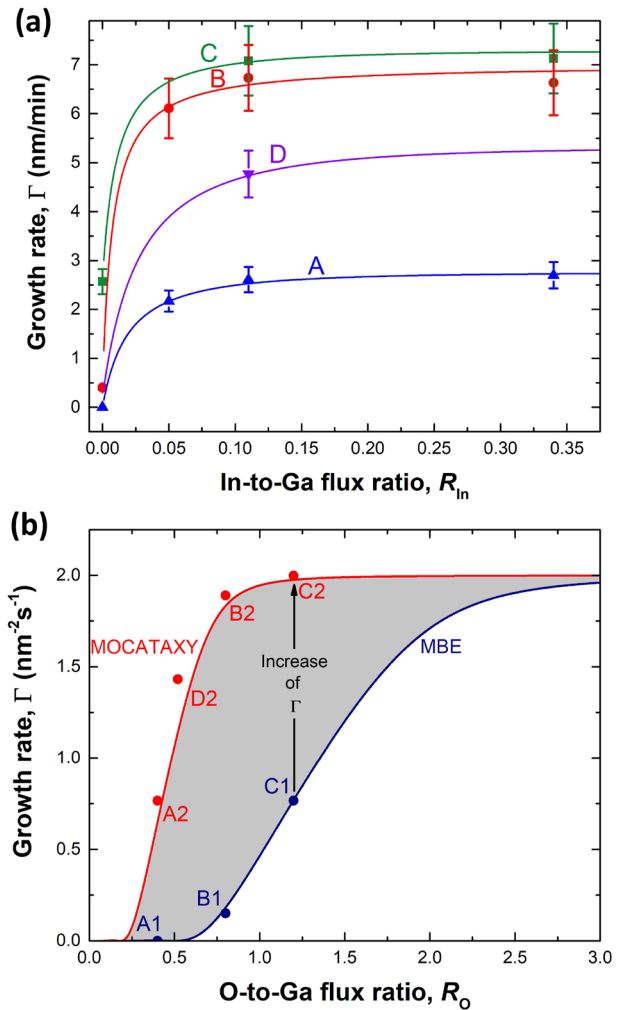**FIG. 1.** (a) Γ in nm min^{-1} as a function of R_{In} at different R_O. Γ measured at R_{In} = 0 corresponds to Ga$_2$O$_3$ growth by MBE and R_{In} > 0 to MOCATAXY. Lines are model calculations[19] and serve as a guide to the eye. (b) MBE and MOCATAXY models for Γ in nm^{-2} s^{-1} as a function of R_O. Models are shown for samples A1–C1 (MBE) and A2–C2 (MOCATAXY). The light-gray-shaded area depicts the expansion of the accessible growth window for α-Ga$_2$O$_3$ grown by MBE and MOCATAXY.

the displayed samples. All layers grown in this study have thicknesses of $d \approx 50$ nm, achieved by adjusting growth time after extracting Γ from calibration growths and consulting the models shown in Fig. 1. For the MBE-grown samples, A1 (R_O = 0.4), B1 (R_O = 0.8), and C1 (R_O = 1.2), at R_{In} = 0, Γ increases with increasing ϕ_O. At the growth conditions of A1, the nucleation and growth of α-Ga$_2$O$_3$ on α-Al$_2$O$_3$(10$\bar{1}$0) is kinetically forbidden, as all active O is consumed to form the volatile suboxide Ga$_2$O, which subsequently desorbs from the α-Al$_2$O$_3$(10$\bar{1}$0) surface. With increasing R_O, the formation of Ga$_2$O becomes less favored, and α-Ga$_2$O$_3$ growth sets in for sample B1, with Γ further increasing for sample C1.

Γ as a function of R_O is shown in Fig. 1(b). The MBE-grown samples (blue points represent experimental Γ and blue line

represents modeled Γ) were grown under Ga-rich conditions, as indicated by the increasing Γ with increasing R_O. Γ plateaus in the O-rich regime, illustrated by the model at $R_O > 1.5$, and becomes limited by the supplied ϕ_{Ga}. To expand the growth window of α-Ga_2O_3, In is additionally supplied to the Ga–O growth system, and MOCATAXY is employed. At the same R_O and T_{TC}, Γ increases with R_{In} [indicated by the arrow in Fig. 1(b)] until Γ plateaus again, now limited by the supplied ϕ_{Ga} and ϕ_{In}.

Our experiment reveals that the available growth window of α-$Ga_2O_3(10\bar{1}0)/\alpha$-$Al_2O_3(10\bar{1}0)$ is widened with larger ϕ_O or ϕ_{In}; see series A ($R_O = 0.4$), B ($R_O = 0.8$), and C ($R_O = 1.2$) in Fig. 1(a). In Fig. 1(b), the light-gray-shaded area and arrow depict the expansion of the accessible growth window for α-Ga_2O_3 grown by MBE and MOCATAXY.

During MOCATAXY, the In as a catalyst provides more active O for metal oxidation to form metal oxides, such as α-Ga_2O_3.[8] Quantitatively, the available ϕ_O for MOCATAXY-grown Ga_2O_3 can be 2.8 times larger than the ϕ_O available for MBE-grown Ga_2O_3.[8,19,21] We note that the models shown in Fig. 1 use arbitrary kinetic parameters, similar to the models shown in Ref. 8. The model closely follows the experimental Γ values as a function of R_O for the MBE and MOCATAXY samples. We find a very good correspondence to the experimental data when assuming full Ga incorporation (2 atoms nm^{-2} s^{-1}) for sample C2 by MOCATAXY, with the higher oxygen flux. It must be noted that the contribution of a 7 met. %

incorporation of In in this sample, as further discussed below, is considered in the model.

B. Surface morphology

The impact of R_{In} and R_O on the surface morphology of the same samples as in Fig. 1 (except A12, B12, and D2) is depicted in Fig. 2. rms roughness is determined by AFM over a 5×5 μm^2 range, shown in the supplementary material, Fig. S1. The corresponding RHEED patterns of all the samples are shown in the insets in Fig. 2. Both samples C2 and C3 exhibit additional weak RHEED spots between the main α-Ga_2O_3-related spots [insets in Figs. 2(f) and 2(c)]. This indicates β-Ga_2O_3 formation, as discussed in the following sections. Rough surfaces (rms $\geq$ 2.3 nm) are observed in MBE samples B1 and C1, whereas the surface rms are improved in the MOCATAXY samples. Samples A2, A3, and D2 [see Fig. S2(a) in the supplementary material] exhibit further improved surface morphologies with lower rms roughnesses (rms $\leq$ 1.9 nm) and extended surface facets. The extended features are oriented parallel to the $[\bar{1}2\bar{1}0]$ (a-plane) direction of α-Ga_2O_3, indicating that In has a pronounced surfactant effect along the $[\bar{1}2\bar{1}0]$ direction with respect to the [0001] direction. The role of In in surface roughening/smoothing [i.e., as a (anti)surfactant] was previously reported during MOCATAXY growth of Ga_2O_3 or $(Al, Ga)_2O_3$.[8,18,31] In acting as a surfactant in the MOCATAXY regime for $R_O \leq 0.53$ may be
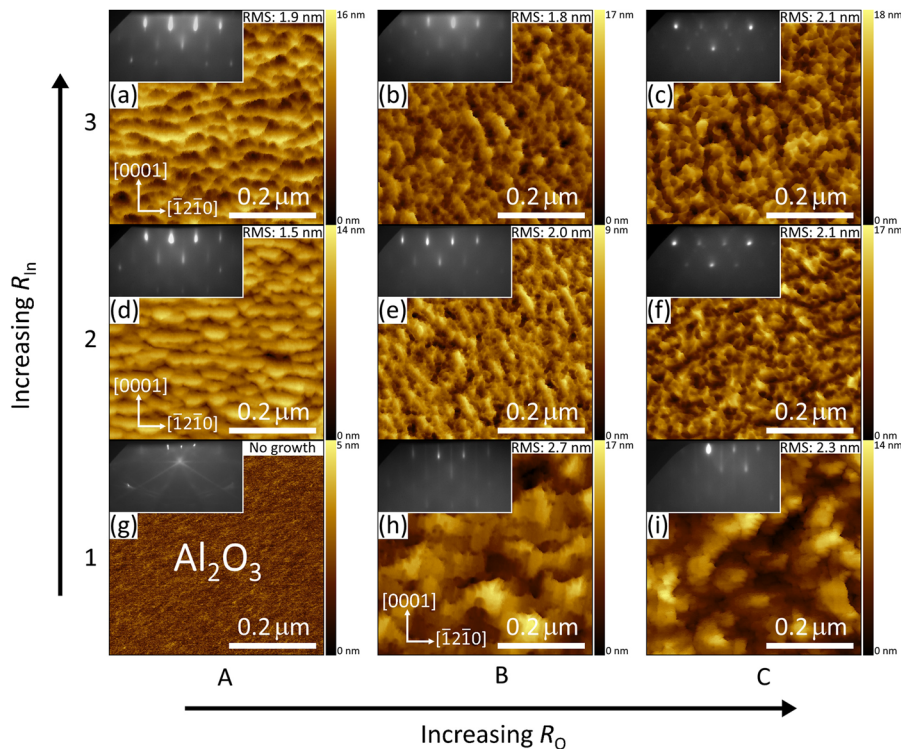

FIG. 2. 0.5×0.5 μm^2 AFM images of samples A1–C3. Insets show corresponding RHEED images, taken along the $[11\bar{2}0]$ azimuth. rms surface roughness values correspond to the 5×5 μm^2 AFM images shown in the supplementary material, Fig. S1.

attributed to enhanced adatom mobility when In is supplied, similar to the well-known In–Ga–N system.[32]

C. Crystalline phase and In incorporation into α-Ga₂O₃

In order to investigate the crystalline phase of the samples in Fig. 2, μ-Raman spectroscopy was employed, as shown in Fig. 3(a). Sample A1 exhibits no Raman modes beyond those of the α-Al₂O₃ substrate[33] (at higher Raman shifts than the displayed range) because no growth has occurred. Samples A2, A3, B1, and C1 all exhibit additional intense and well-defined Raman peaks at 217 and 285 cm⁻¹, which are characteristic modes of the corundum α-Ga₂O₃ structure.[34] In samples B2, B3, C2, and C3, the peak positions of the corundum Raman modes present much lower relative intensities, higher full widths at half maximum (FWHM, e.g., 11 cm⁻¹ for the 217 cm⁻¹ peak in sample B2, compared to 5 cm⁻¹ in lower ϕ_O and ϕ_{In} samples), and Raman redshifts, which can be explained by the substantial amount of In in these α-Ga₂O₃ films,
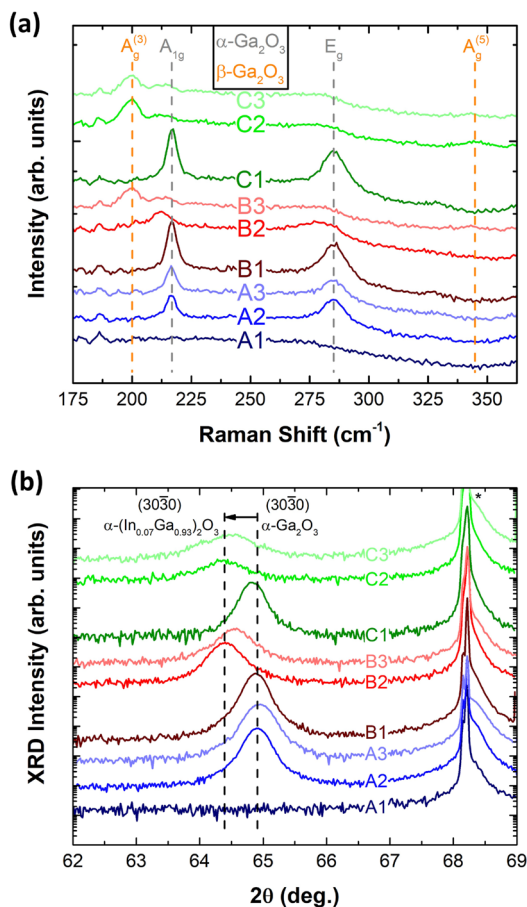

(a)

(b)

FIG. 3. (a) μ-Raman spectra acquired for samples A1–C3, with α-Ga₂O₃ and β-Ga₂O₃ Raman modes marked by gray and orange dashed lines, respectively. (b) Symmetric $2\theta - \omega$ HRXRD scans recorded for samples A1–C3. The peak of the α-Al₂O₃ substrate is marked by an asterisk. The α-(In$_x$Ga$_{1-x}$)₂O₃ peaks are marked by dashed lines for $x = 0.07$ and $x = 0$.

in agreement with In concentrations extracted from HRXRD discussed below. In addition, all of these samples except B2 display intense peaks at Raman shifts of 199–200 and 344 cm⁻¹, which are assigned to the $A_g^{(3)}$ and $A_g^{(5)}$ modes of monoclinic β-(In)Ga₂O₃, respectively.[35,36] This reveals the presence of β-(In$_x$Ga$_{1-x}$)₂O₃ in the MOCATAXY samples when high R_{In} and R_O are provided. It should be noted that trial growths with lower thicknesses result in phase-pure α-(In$_x$Ga$_{1-x}$)₂O₃ layers, which implies that β-(In$_x$Ga$_{1-x}$)₂O₃ heteroepitaxially grows on α-(In$_x$Ga$_{1-x}$)₂O₃ after a critical thickness. This is investigated further in Sec. III D.

Figure 3(b) shows symmetric $2\theta - \omega$ HRXRD scans. No (30$\bar{3}$0) α-Ga₂O₃ reflex is detectable in sample A1, as the nucleation and growth of Ga₂O₃ are kinetically forbidden. Samples grown by MBE with larger ϕ_O (B1, C1) exhibit the expected (30$\bar{3}$0) α-Ga₂O₃ reflex at $2\theta = 64.9°$.[3,8] No other crystalline phases of Ga₂O₃ were detected. However, MOCATAXY samples grown with $R_{In} \geq 0.11$ and $R_O \geq 0.80$ (samples B2 and B3, C2 and C3) show a shift in the diffraction angles to $2\theta = 64.4°$–$64.6°$ due to In incorporation in the α-Ga₂O₃ layer, while those with $R_O \leq 0.53$ (samples A2, D2, and A3) still exhibit the (30$\bar{3}$0) reflex at $64.9°$ [see the blue spectrum and Fig. S2(b)].

For fully relaxed films, Vegard's law for the a-lattice parameter may be used to extract In concentrations from diffraction peak positions. From HRXRD, the average In concentration in the α-(In$_x$Ga$_{1-x}$)₂O₃ samples is estimated to be $x \approx 0.07$ for sample B2. No strain is considered for this estimation, as a reciprocal space map (RSM), shown in Fig. S3 in the supplementary material, shows the layer to be fully relaxed. An independent concentration determination using STEM-EDX yielded $x = 0.07 \pm 0.01$ [see Fig. S6(b)], which is in good agreement with this result. Once ϕ_{In} is further increased at constant R_O, a gradual shift to higher 2θ angles, up to $64.7°$ in samples B2–B4, is observed (see Fig. S4), i.e., a lower In incorporation is measured, down to $x \approx 0.03$, despite a higher R_{In} supplied. We attribute this behavior to the In solubility limit in α-Ga₂O₃ being reached for our growth conditions and the excess In forming the suboxide In₂O that may desorb from the growth surface at these metal-rich flux conditions. A recent investigation in ε-(In$_x$Ga$_{1-x}$)₂O₃ found analogous behavior at high ϕ_{In}, with In concentrations approaching $x \approx 0$.[31] The maximum In concentration of $x \approx 0.08$ in sample B2 agrees with the reported maximum In concentration for mist CVD-grown phase-pure α-(In$_x$Ga$_{1-x}$)₂O₃.[37] In contrast, MOCATAXY-grown samples A2, A3, and D2 [blue spectra in Fig. 3 and Fig. S2(b) in the supplementary material] are phase-pure α-Ga₂O₃ and have lower surface rms roughnesses. This effect can be correlated with the thermodynamics of the In incorporation in β-(In$_x$Ga$_{1-x}$)₂O₃, reported in Ref. 14. There, it was found that a low metal-to-oxygen flux ratio (R_{Me}) leads to β-(In$_x$Ga$_{1-x}$)₂O₃, while β-Ga₂O₃ was obtained when $R_{Me} = (\phi_{In} + \phi_{Ga})/\phi_O = 2$. This is also the case here; sample D2 was grown with $R_{Me} = 2.1$ and no observable In incorporation, while sample B2 (red spectrum in Fig. 3), with $R_{Me} = 1.4$, contains ∼7% In.

Rocking curves for representative samples can be found in the supplementary material, Fig. S5. The MBE-grown α-Ga₂O₃ (B1 and C1) and the MOCATAXY-grown α-Ga₂O₃ (A2) samples exhibit the same FWHM, suggesting MOCATAXY does not provide a measurable improvement in the mosaicity at these growth conditions. In contrast, α-(In$_x$Ga$_{1-x}$)₂O₃ samples [e.g., B2 in Fig. S5(c)] show

markedly increased FWHM values, due to varying In concentrations within layers and greater mosaic spreads.

The AFM and HRXRD data suggest $R_{Me} \geq 2$ is required to take full advantage of In being a catalyst and surfactant for the growth of α-Ga_2O_3. Conditions with $R_{Me} < 2$ result in the sub-optimal role of In as a surfactant with In incorporation in the layer up to its solubility limit, while too high R_{Me} results in no growth. These R_{Me}-dependent behaviors closely follow those observed for β-Ga_2O_3.[14]

D. Faceting and interfaces

To identify the mechanisms leading to β-$(In_xGa_{1-x})_2O_3$ heteroepitaxial growth or phase-pure α-Ga_2O_3 on α-$Al_2O_3(10-10)$, skew-symmetric HRXRD scans and STEM analysis were performed. In Fig. 4(a), skew-symmetric HRXRD ϕ-scans at $\chi = 30°$ (i.e., parallel to the a-plane of α-Al_2O_3) for a sample equivalent to C3, but with $d = 390$ nm to maximize β-Ga_2O_3 growth and signal, are shown. The diffraction peaks of a-plane $(2\bar{1}\bar{1}0)$ α-Al_2O_3 and α-$(In_xGa_{1-x})_2O_3$ are measured since the $(2\bar{1}\bar{1}0)$ plane forms $30°$ with respect to the growth plane $(10\bar{1}0)$. In addition, the $(\bar{6}03)$ β-$(In_xGa_{1-x})_2O_3$ reflex at $2\theta = 59.2°$ is clearly visible in this orientation. Hence, the α-Al_2O_3 substrate, the initial α-$(In_xGa_{1-x})_2O_3$ film, and the subsequent β-$(In_xGa_{1-x})_2O_3$ layer are identified with the epitaxial relationship $(\bar{2}01)$ β-$(In_xGa_{1-x})_2O_3 \parallel (2\bar{1}\bar{1}0)$ α-$(In_xGa_{1-x})_2O_3$. Both $(2\bar{1}\bar{1}0)$ planes in Fig. 4(a) show two-fold symmetry in the $360°$ ϕ scan and appear at the same ϕ angle, which implies that there are no rotational domains in the α-$(In,Ga)_2O_3$ layer (nor in the α-Ga_2O_3 samples) on m-plane α-Al_2O_3.[38]

Figure 4(b) shows a cross-sectional HAADF overview and magnified images of sample C3. Two distinct phases are identified: α-$(In_xGa_{1-x})_2O_3$ [see below solid orange lines in Fig. 4(b)] and β-$(In_xGa_{1-x})_2O_3$ [see above dashed orange lines in Fig. 4(b)]. The $(2\bar{1}\bar{1}0)$ facet of the α-phase is identified as the growth surface for β-$(In_xGa_{1-x})_2O_3$. In the HAADF image, we could only resolve the atomic distances between $(\bar{2}01)$ planes of β-$(In_xGa_{1-x})_2O_3$, but not perpendicular distances. We expect that these perpendicular distances should be resolvable in [010] and [132]-type orientations. Therefore, the most likely epitaxial relation between α-$(In_xGa_{1-x})_2O_3$ and β-$(In_xGa_{1-x})_2O_3$ is $(\bar{2}01)$ β-$(In_xGa_{1-x})_2O_3$ $\parallel$ $(2\bar{1}\bar{1}0)$ α-$(In_xGa_{1-x})_2O_3$ and [102] β-$(In_xGa_{1-x})_2O_3$ $\parallel$ [0001] α-$(In_xGa_{1-x})_2O_3$. Hence, at a film thickness $d \approx 50$ nm, nucleation of the β-phase only occurs in the MOCATAXY region when there is a sufficiently large R_O and R_{In} that allow for In incorporation. STEM-EDX is shown for sample C3 in the supplementary material, Fig. S6(a). Delayed In incorporation is observed in the film. The maximum concentration of In measured in C3, $x \approx 0.12$, occurs after $d \approx 25$ nm. Accordingly, this higher In incorporation occurs in β-Ga_2O_3. Higher metal concentrations of In in β-$(In_xGa_{1-x})_2O_3$ were previously theoretically predicted[39] and experimentally achieved by MBE.[40]

Cross-sectional HAADF images and STEM-EDX for sample B2 are shown in the supplementary material, Figs. S6(b) and S7 $(2\bar{1}\bar{1}0)$. a-plane facets are also identified in this sample, without the growth of β-$(In_xGa_{1-x})_2O_3$, suggesting that the critical α-$(In_xGa_{1-x})_2O_3$ thickness before β-Ga_2O_3 nucleation is about to be reached for these growth conditions. Such critical thickness, $d \approx 50$ nm, is double that of, e.g., sample C3, which implies that the a-plane facet formation
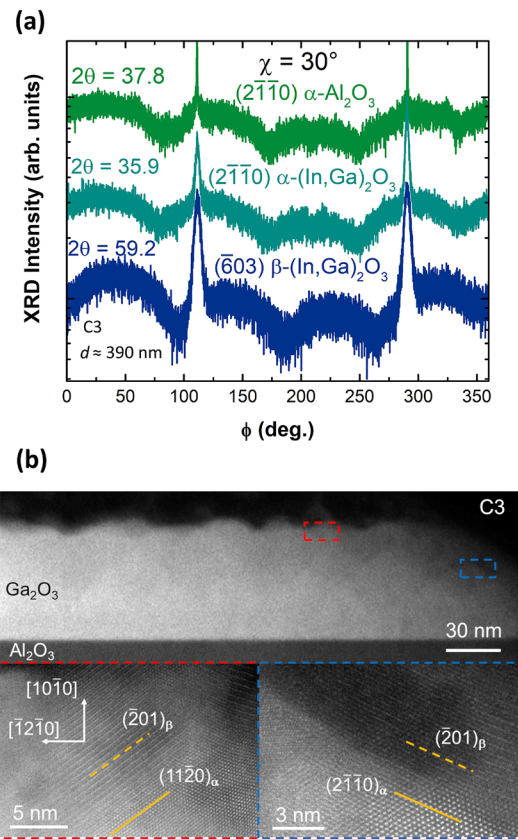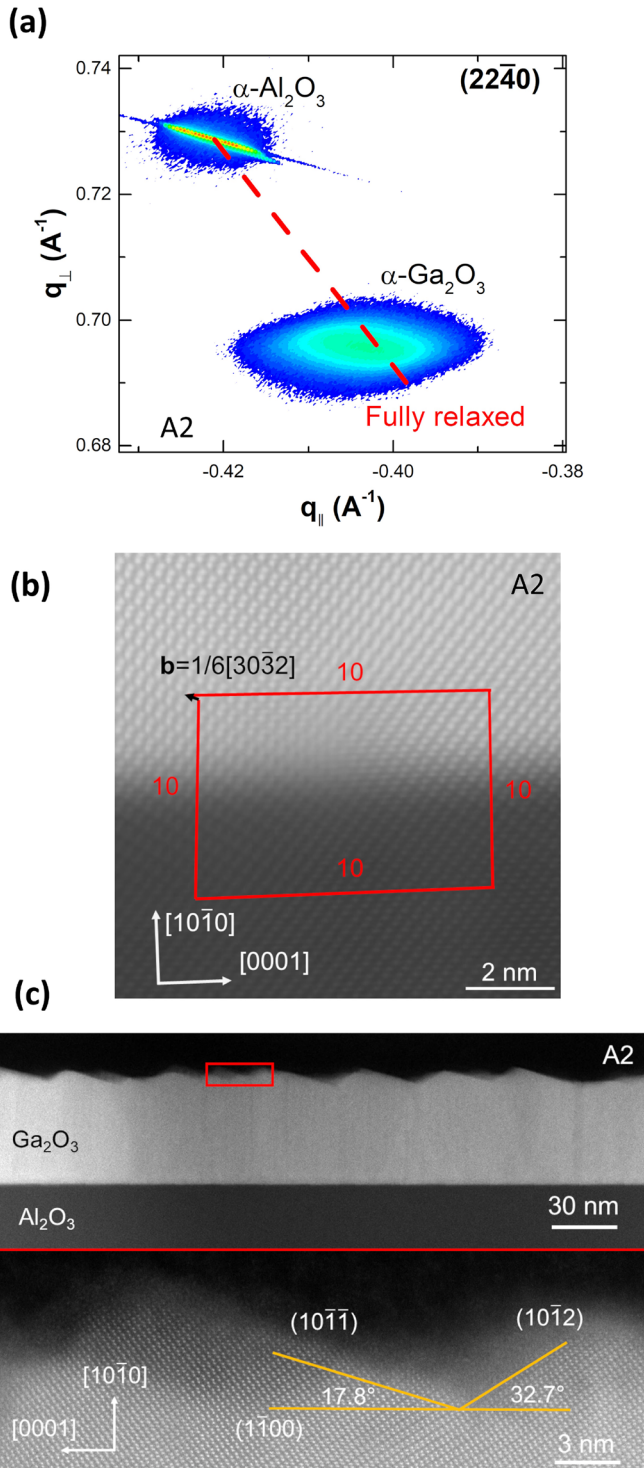

FIG. 4. Sample C3: (a) For a film with $d \approx 390$ nm, skew-symmetric HRXRD ϕ scans ($\chi = 30°$) of the $(2\bar{1}\bar{1}0)$ peak of the α-Al_2O_3 substrate, the $(2\bar{1}\bar{1}0)$ peak of α-$(In_xGa_{1-x})_2O_3$, and the $(\bar{6}03)$ peaks of β-$(In_xGa_{1-x})_2O_3$. (b) Cross-sectional HAADF overview and magnified images, showing two examples of the a-plane faceting and its epitaxial relation to $(\bar{2}01)$ β-$(In_xGa_{1-x})_2O_3$.

and subsequent β-$(In_xGa_{1-x})_2O_3$ growth are delayed when reducing R_{In} to 0.11 and R_O to 0.8.

An HRXRD RSM of sample A2 around the $(22\bar{4}0)$ α-Ga_2O_3 reflex is shown in Fig. 5(a). The dashed line intersects the fully-relaxed α-Al_2O_3 and α-Ga_2O_3 reciprocal lattice points. The results indicate that the 50 nm α-Ga_2O_3 layer is fully relaxed. Figure 5(b) shows the substrate-film interface in sample A2, with the presence of a misfit dislocation. The film relaxes at the interface to reduce the elastic strain energy between $Ga_2O_3(10\bar{1}0)$ and $Al_2O_3(10\bar{1}0)$.[41] The magnitude of the dislocation shown in Fig. 5(b) can be represented by the Burgers vector $\mathbf{b} = 1/6[30\bar{3}2]$.

Figure 5(c) shows the cross-sectional HAADF overview and magnified images at the surface of sample A2. Single-crystalline material is identified in the observed regions over the range of a few microns. Unlike sample C3, no a-plane facets or secondary phase formation are present in A2. Instead $(10\bar{1}1)$, facets are observed on the surface, reflecting the morphology observed by AFM. The equivalency of $Ga_2O_3(10\bar{1}1)$ and $Ga_2O_3(10\bar{1}\bar{1})$, due to symmetry, confirms the noted surface facet orientation we previously reported.[8] STEM-EDX cross-sectional maps and line scans for sample A2 are

(a)

(b)

(c)

FIG. 5. Sample A2: (a) RSM ($q_\parallel$, $q_\perp$) around the ($22\bar{4}0$) reflex of sample A2, displaying full relaxation of the α-Ga$_2$O$_3$ film. (b) Magnified cross-sectional HAADF image of the substrate-layer interface, with the Burgers vector **b** noted. (c) Cross-sectional HAADF overview and magnified images, showing the formation of ($10\bar{1}1$) and ($11\bar{1}2$) facets, indicated in yellow.

shown in the supplementary material, Fig. S6(c). In accordance with the HRXRD and μ-Raman analysis, In does not substantially incorporate in the film, i.e., below 1 at. %.

E. MBE and MOCATAXY phase diagram of Ga$_2$O$_3$

To guide the growth of α-Ga$_2$O$_3$($10\bar{1}0$)/α-Al$_2$O$_3$($10\bar{1}0$), Fig. 6(a) shows a phase diagram that encompasses the $d \approx 50$ nm films studied in this work (Table II). Up to this thickness, only MOCATAXY-grown samples with high R_{In} and high R_O exhibit heteroepitaxial β-(In$_x$Ga$_{1-x}$)$_2$O$_3$ growth. At lower $R_{In} = 0.05$ and

(a)

(b)

FIG. 6. (a) Measured and developed growth and phase diagram of α-(In$_x$Ga$_{1-x}$)$_2$O$_3$ with $x \leq 0.08$ at $T_{TC} = 775\,^\circ$C, $\phi_{Ga} = 4.0$ nm^{-2} s^{-1} and $d \approx 50$ nm, projected onto the two-dimensional parameter space spanned by the In-to-Ga flux ratio (R_{In}) and O-to-Ga flux ratio (R_O). Four major regimes are indicated: (i) no growth, (ii) single-crystalline α-Ga$_2$O$_3$, (iii) phase-pure α-(In$_x$Ga$_{1-x}$)$_2$O$_3$, and (iv) α-(In$_x$Ga$_{1-x}$)$_2$O$_3$ and β-(In$_x$Ga$_{1-x}$)$_2$O$_3$ growth regimes. (b) Schematic of Ga$_2$O$_3$ phase growth and faceting on m-plane α-Al$_2$O$_3$, for different R_{In} and R_O, and $d = 50$ nm. The epitaxial relationships are shown by an illustration on the right side of the figure. Light gray lines serve as a guide to the eye in Fig. 6(a).

R_O = 0.80 [see Fig. S2(a)], In also incorporates into the grown layers, but no secondary β-phase is observed. In that sample, the solubility limit of In ($x \approx 0.08$) in α-Ga_2O_3 is already reached. For $R_O \leq 0.53$, independent of R_{In}, phase-pure α-Ga_2O_3, layers with In incorporation below 1 at. % are obtained.

Figure 6(b) sketches the growth-parameter-dependent α-Ga_2O_3 surface faceting and α-$(In_xGa_{1-x})_2O_3$-to-β-$(In_xGa_{1-x})_2O_3$ phase transition critical thickness for our d = 50 nm samples. It is possible to achieve single-crystalline α-Ga_2O_3 both by MBE and MOCATAXY. For the latter, it is necessary to supply a relatively low oxygen flux, $R_O \leq 0.53$. Under such conditions $(10\bar{1}1)$, plane facets appear on the α-Ga_2O_3 surface, similar to what was reported in Ref. 8. It must be noted that, similar to a recent PLD study on α-Ga_2O_3,[12] we have detected inhomogeneous β-(In)Ga_2O_3 formation on thicker (> 100 nm) samples under these growth conditions, which is an open topic beyond the scope of this work. Our results assert the need to tune the growth parameters, aiming for smooth layer-by-layer growth that prevents the formation of facets where the secondary phase growth takes place. This is partially achieved in the A2 sample at T_{TC} = 825 °C, as presented in Sec. III F.

F. Temperature-dependent growth series

To investigate the effect of T_{TC} on our optimized phase-pure α-Ga_2O_3 film (sample A2), a T_{TC}-series at such optimal ϕ_{Ga}, ϕ_{In},

and ϕ_O is performed. Figure 7(a) shows a decrease in Γ with increasing T_{TC} due to increased Ga_2O desorption.[13] The rocking curve for the sample grown at T_{TC} = 825 °C is shown in the supplementary material, Fig. S5(e), indicating an improvement in the layer's mosaicity with respect to the equivalent sample at T_{TC} = 775 °C, Fig. S5(a). Figures 7(b) and 7(c) show 5 × 5 μm^2 and 0.5 × 0.5 μm^2 AFM images of the sample grown at 825 °C. Its surface exhibits well-defined terraces and step edges, also observable by the modulated streaky RHEED pattern. The step size can vary by a significant amount across the surface, with most falling in the range of 3–5 nm, corresponding to ~14–23 atomic planes. Again, as revealed by AFM and HRXRD, these features are aligned parallel to the $[\bar{1}2\bar{1}0]$ direction [marked in Figs. 7(b) and 7(c)]. Although the surface rms roughness of this sample is higher than the value for sample A2 (same conditions but T_{TC} = 775 °C), certain areas such as the one shown in Fig. 7(c) possess markedly lower rms values of 1.0–1.3 nm, pointing toward the possibility of achieving smoother α-Ga_2O_3 thin films at this T_{TC}. The drastic T_{TC}-driven surface morphology change with respect to sample A2 can be attributed to enhanced adatom surface mobility.

As shown in the symmetric HRXRD spectrum of the $(30\bar{3}0)$ reflex of these T_{TC}-dependent samples in Fig. S8, no additional phases and no α-Ga_2O_3 peak shifts above the experimental uncertainty were present, which indicates the dominant role of the In–Ga–O kinetics with respect to thermodynamics in the formation of phase-pure α-Ga_2O_3.

IV. CONCLUSIONS

The effect of varying the In and O fluxes on the formation of α-Ga_2O_3 on m-plane α-Al_2O_3 by MBE has been systematically investigated. Using MOCATAXY, three growth regimes are identified, resulting in: (i) single-crystalline α-Ga_2O_3, (ii) phase-pure α-$(In_xGa_{1-x})_2O_3$, with up to x = 0.07 ± 0.01, and (iii) α-$(In_xGa_{1-x})_2O_3$ + β-$(In_xGa_{1-x})_2O_3$ growth on a-plane α-$(In_xGa_{1-x})_2O_3$ facets. To grow single-crystalline α-Ga_2O_3 by In-assisted MOCATAXY and avoid considerable In incorporation, $R_O \leq 0.53$ is necessary. Under these conditions, In acts as a surfactant along the $[\bar{1}2\bar{1}0]$ direction. Higher T_{TC} results in step-like growth, with the potential to achieve smoother α-Ga_2O_3 samples that prevent secondary phase formation in thicker films. Such understanding and optimization of the growth kinetics and thermodynamics of α-Ga_2O_3 on α-Al_2O_3 is necessary in order to realize high quality films and heterostructures based on this ultra-wide bandgap material system.

SUPPLEMENTARY MATERIAL

Additional data that support the findings of this work, referenced in the main text as S1–S8, is provided in the supplementary material.
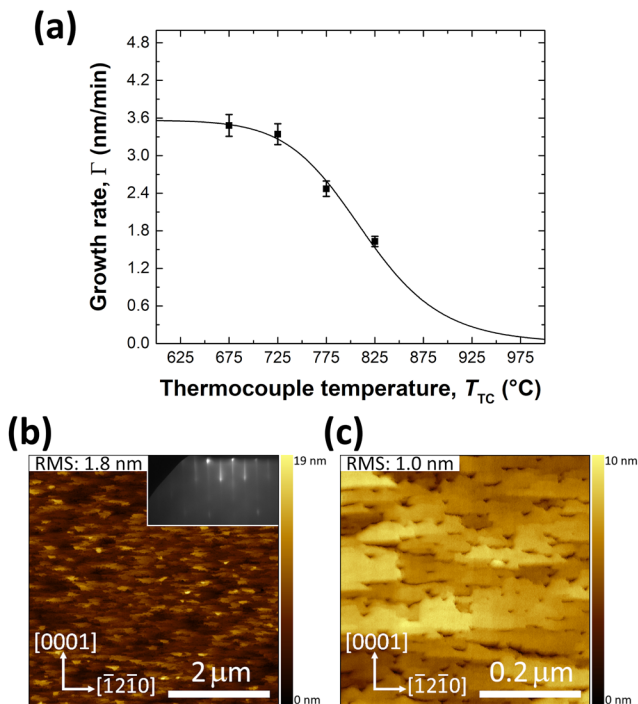
ACKNOWLEDGMENTS

FIG. 7. (a) Temperature-dependent growth rate for samples grown with parameters of A2; line fit is a model fit and serves as a guide to the eye. (b) 5 × 5 μm^2 AFM image of A2 grown at 825 °C, inset shows RHEED pattern taken along [11$\bar{2}$0] azimuth, and (c) 500 × 500 nm^2 AFM image of the same sample, exhibiting well-defined terraces and step edges.

AUTHOR DECLARATIONS

Conflict of Interest

The authors have no conflicts to disclose.

Author Contributions

M.S.W. and M.A.-O. contributed equally to this work.

Martin S. Williams: Conceptualization (equal); Data curation (lead); Formal analysis (lead); Investigation (lead); Methodology (equal); Writing – original draft (lead); Writing – review & editing (lead). **Manuel Alonso-Orts**: Conceptualization (lead); Data curation (equal); Formal analysis (equal); Methodology (equal); Project administration (lead); Supervision (lead); Writing – original draft (lead); Writing – review & editing (lead). **Marco Schowalter**: Data curation (equal); Formal analysis (equal); Writing – original draft (equal); Writing – review & editing (supporting). **Alexander Karg**: Investigation (supporting); Writing – review & editing (supporting). **Sushma Raghuvansy**: Investigation (supporting). **Jon P. McCandless**: Conceptualization (supporting); Writing – review & editing (supporting). **Debdeep Jena**: Conceptualization (supporting). **Andreas Rosenauer**: Resources (equal); Writing – review & editing (supporting). **Martin Eickhoff**: Formal analysis (supporting); Funding acquisition (lead); Project administration (supporting); Resources (lead); Supervision (equal); Writing – review & editing (supporting). **Patrick Vogt**: Conceptualization (equal); Data curation (equal); Formal analysis (equal); Methodology (lead); Project administration (lead); Supervision (equal); Writing – original draft (supporting); Writing – review & editing (lead).

DATA AVAILABILITY

The data that support the findings of this study are available from the corresponding author upon reasonable request.

REFERENCES

[1] C. Venkata Prasad and Y. S. Rim, "Review on interface engineering of low leakage current and on-resistance for high-efficiency Ga_2O_3-based power devices," Mater. Today Phys. **27**, 100777 (2022).

[2] S. B. Reese, T. Remo, J. Green, and A. Zakutayev, "How much will gallium oxide power electronics cost?," Joule **3**, 903 (2019).

[3] R. Jinno, C. S. Chang, T. Onuma, Y. Cho, S.-T. Ho, D. Rowe, M. C. Cao, K. Lee, V. Protasenko, D. G. Schlom, D. A. Muller, H. G. Xing, and D. Jena, "Crystal orientation dictated epitaxy of ultrawide-bandgap 5.4–8.6-eV α-(AlGa)$_2$O$_3$ on m-plane sapphire," Sci. Adv. **7**, eabd5891 (2021).

[4] J. P. McCandless, C. S. Chang, K. Nomoto, J. Casamento, V. Protasenko, P. Vogt, D. Rowe, K. Gann, S. T. Ho, W. Li, R. Jinno, Y. Cho, A. J. Green, K. D. Chabak, D. G. Schlom, M. O. Thompson, D. A. Muller, H. G. Xing, and D. Jena, "Thermal stability of epitaxial α-Ga$_2$O$_3$ and (Al, Ga)$_2$O$_3$ layers on m-plane sapphire," Appl. Phys. Lett. **119**, 062102 (2021).

[5] E. Ahmadi, O. S. Koksaldi, X. Zheng, T. Mates, Y. Oshima, U. K. Mishra, and J. S. Speck, "Demonstration of β-(Al, Ga)$_2$O$_3$/β-Ga$_2$O$_3$ modulation doped field-effect transistors with Ge as dopant grown via plasma-assisted molecular beam epitaxy," Appl. Phys. Express **10**, 071101 (2017).

[6] A. F. M. A. U. Bhuiyan, Z. Feng, J. M. Johnson, H. L. Huang, J. Sarker, M. Zhu, M. R. Karim, B. Mazumder, J. Hwang, and H. Zhao, "Phase transformation in MOCVD growth of (Al, Ga)$_2$O$_3$ thin films," APL Mater. **8**, 031104 (2020).

[7] M. Kracht, A. Karg, M. Feneberg, J. Bläsing, J. Schörmann, R. Goldhahn, and M. Eickhoff, "Anisotropic optical properties of metastable (01–12) α-Ga$_2$O$_3$ grown by plasma-assisted molecular beam epitaxy," Phys. Rev. Appl. **10** 024047 (2018),

[8] J. P. McCandless, D. Rowe, N. Pieczulewski, V. Protasenko, M. Alonso-Orts, M. S. Williams, M. Eickhoff, H. G. Xing, D. A. Muller, D. Jena, and P. Vogt, "Growth of α-Ga$_2$O$_3$ on α-Al$_2$O$_3$ by conventional molecular-beam epitaxy and metal-oxide-catalyzed epitaxy," Jpn. J. Appl. Phys. **62**, SF1013 (2023).

[9] G. T. Dang, T. Yasuoka, Y. Tagashira, T. Tadokoro, W. Theiss, and T. Kawaharamura, "Bandgap engineering of α-(Al$_x$Ga$_{1-x}$)$_2$O$_3$ by a mist chemical vapor deposition two-chamber system and verification of Vegard's law," Appl. Phys. Lett. **113**, 062102 (2018).

[10] K. Uno, M. Ohta, and I. Tanaka, "Growth mechanism of α-Ga$_2$O$_3$ on a sapphire substrate by mist chemical vapor deposition using acetylacetonated gallium source solutions," Appl. Phys. Lett. **117**, 052106 (2020).

[11] M. Kneiß, D. Splith, H. von Wenckstern, M. Lorenz, T. Schultz, N. Koch, and M. Grundmann, "Strain states and relaxation for α-(Al$_x$Ga$_{1-x}$)$_2$O$_3$ thin films on prismatic planes of α-Al$_2$O$_3$ in the full composition range: Fundamental difference of a- and m-epitaxial planes in the manifestation of shear strain and lattice tilt," J. Mater. Res. **36**, 4816 (2021).

[12] C. Petersen, S. Vogt, M. Kneiß, H. von Wenckstern, and M. Grundmann, "PLD of α-Ga$_2$O$_3$ on m-plane Al$_2$O$_3$: Growth regime, growth process, and structural properties," APL Mater. **11**, 061122 (2023).

[13] P. Vogt and O. Bierwagen, "Quantitative subcompound-mediated reaction model for the molecular beam epitaxy of III–VI and IV–VI thin films: Applied to Ga$_2$O$_3$, In$_2$O$_3$, and SnO$_2$," Phys. Rev. Mater. **2**, 120401 (2018).

[14] P. Vogt and O. Bierwagen, "Kinetics versus thermodynamics of the metal incorporation in molecular beam epitaxy of (In$_x$Ga$_{1-x}$)$_2$O$_3$," APL Mater. **4**, 086112 (2016).

[15] P. Vogt, F. V. Hensling, K. Azizie, C. S. Chang, D. Turner, J. Park, J. P. McCandless, H. Paik, B. J. Bocklund, G. Hoffman, O. Bierwagen, D. Jena, H. G. Xing, S. Mou, D. A. Muller, S. L. Shang, Z. K. Liu, and D. G. Schlom, "Adsorption-controlled growth of Ga$_2$O$_3$ by suboxide molecular-beam epitaxy," APL Mater. **9**, 031101 (2021).

[16] S. Lany, "Defect phase diagram for doping of Ga$_2$O$_3$," APL Mater. **6**, 046103 (2018).

[17] E. Korhonen, F. Tuomisto, D. Gogova, G. Wagner, M. Baldini, Z. Galazka, R. Schewski, and M. Albrecht, "Electrical compensation by Ga vacancies in Ga$_2$O$_3$ thin films," Appl. Phys. Lett. **106**, 242103 (2015).

[18] P. Vogt, A. Mauze, F. Wu, B. Bonef, and J. S. Speck, "Metal-oxide catalyzed epitaxy (MOCATAXY): The example of the O plasma-assisted molecular beam epitaxy of β-(Al$_x$Ga$_{1-x}$)$_2$O$_3$/β-Ga$_2$O$_3$ heterostructures," Appl. Phys. Express **11**, 115503 (2018).

[19] P. Vogt, O. Brandt, H. Riechert, J. Lähnemann, and O. Bierwagen, "Metal-exchange catalysis in the growth of sesquioxides: Towards heterostructures of transparent oxide semiconductors," Phys. Rev. Lett. **119**, 196001 (2017).

[20] M. Kracht, A. Karg, J. Schörmann, M. Weinhold, D. Zink, F. Michel, M. Rohnke, M. Schowalter, B. Gerken, A. Rosenauer, P. J. Klar, J. Janek, and M. Eickhoff, "Tin-assisted synthesis of ε-Ga$_2$O$_3$ by molecular beam epitaxy," Phys. Rev. Appl. **8**, 054002 (2017).

[21] P. Vogt, F. V. Hensling, K. Azizie, J. P. McCandless, J. Park, K. Delello, D. A. Muller, H. G. Xing, D. Jena, and D. G. Schlom, "Extending the kinetic and thermodynamic limits of molecular-beam epitaxy utilizing suboxide sources or metal-oxide-catalyzed epitaxy," Phys. Rev. Appl. **17**, 034021 (2022).

[22] P. Mazzolini, P. Vogt, R. Schewski, C. Wouters, M. Albrecht, and O. Bierwagen, "Faceting and metal-exchange catalysis in (010) β-Ga$_2$O$_3$ thin films homoepitaxially grown by plasma-assisted molecular beam epitaxy," APL Mater. **7**, 022511 (2018).

[23] A. Mauze, Y. Zhang, T. Itoh, F. Wu, and J. S. Speck, "Metal oxide catalyzed epitaxy (MOCATAXY) of β-Ga$_2$O$_3$ films in various orientations grown by plasma-assisted molecular beam epitaxy," APL Mater. **8**, 021104 (2020).

[24]P. Mazzolini, A. Falkenstein, C. Wouters, R. Schewski, T. Markurt, Z. Galazka, M. Martin, M. Albrecht, and O. Bierwagen, "Substrate-orientation dependence of β-Ga$_2$O$_3$ (100), (010), (001), and (201) homoepitaxy by indium-mediated metal-exchange catalyzed molecular beam epitaxy (MEXCAT-MBE)," APL Mater. **8**, 011107 (2020).

[25]R. Schewski, G. Wagner, M. Baldini, D. Gogova, Z. Galazka, T. Schulz, T. Remmele, T. Markurt, H. von Wenckstern, M. Grundmann *et al.*, "Epitaxial stabilization of pseudomorphic α-Ga$_2$O$_3$ on sapphire (0001)," Appl. Phys. Express **8**, 011101 (2015).

[26]Z. Cheng, M. Hanke, P. Vogt, O. Bierwagen, and A. Trampert, "Phase formation and strain relaxation of Ga$_2$O$_3$ on c-plane and a-plane sapphire substrates as studied by synchrotron-based x-ray diffraction," Appl. Phys. Lett. **111**, 162104 (2017).

[27]A. Karg, J. A. Bich, A. Messow, M. Schowalter, S. Figge, A. Rosenauer, P. Vogt, and M. Eickhoff, "Nucleation window of Ga$_2$O$_3$ and In$_2$O$_3$ for molecular beam epitaxy on (0001) Al$_2$O$_3$," Cryst. Growth Des. **23**, 4435 (2023).

[28]P. Vogt, "Growth kinetics, thermodynamics, and phase formation of group-III and IV oxides during molecular beam epitaxy," Ph.D. thesis, Humboldt-Universität zu Berlin, Berlin (2017).

[29]R. H. Lamoreaux, D. L. Hildenbrand, and L. Brewer, "High-temperature vaporization behavior of oxides II. Oxides of Be, Mg, Ca, Sr, Ba, B, Al, Ga, in, Tl, Si, Ge, Sn, Pb, Zn, Cd, and Hg," J. Phys. Chem. Ref. Data **16**, 419 (1987).

[30]K. Momma and F. Izumi, "*VESTA3* for three-dimensional visualization of crystal, volumetric and morphology data," J. Appl. Crystallogr. **44**, 1272 (2011).

[31]A. Karg, A. Hinz, S. Figge, M. Schowalter, P. Vogt, A. Rosenauer, and M. Eickhoff, "Indium: A surfactant for the growth of ϵ/κ-Ga$_2$O$_3$ by molecular beam epitaxy," APL Mater. **11**, 091114 (2023).

[32]J. Neugebauer, T. K. Zywietz, M. Scheffler, J. E. Northrup, H. Chen, and R. M. Feenstra, "Adatom kinetics on and below the surface: The existence of a new diffusion channel," Phys. Rev. Lett. **90**, 056101 (2003).

[33]V. Palanza, D. Di Martino, A. Paleari, G. Spinolo, and L. Prosperi, "Micro-Raman spectroscopy applied to the study of inclusions within sapphire," J. Raman Spectrosc. **39**, 1007 (2008).

[34]R. Cuscó, N. Domènech-Amador, T. Hatakeyama, T. Yamaguchi, T. Honda, and L. Artús, "Lattice dynamics of a mist-chemical vapor deposition-grown corundum-like Ga$_2$O$_3$ single crystal," J. Appl. Phys. **117**, 185706 (2015).

[35]S. Kumar, G. Sarau, C. Tessarek, M. Y. Bashouti, A. Hähnel, S. Christiansen, and R. Singh, "Study of iron-catalysed growth of β-Ga$_2$O$_3$ nanowires and their detailed characterization using TEM, Raman and cathodoluminescence techniques," J. Phys. D: Appl. Phys. **47**, 435101 (2014).

[36]C. Kranert, C. Sturm, R. Schmidt-Grund, and M. Grundmann, "Raman tensor elements of β-Ga$_2$O$_3$," Sci. Rep. **6**, 35964 (2016).

[37]N. Suzuki, K. Kaneko, and S. Fujita, "Growth of corundum-structured (In$_x$Ga$_{1-x}$)$_2$O$_3$ alloy thin films on sapphire substrates with buffer layers," J. Cryst. Growth **401**, 670 (2014), part of Special Issue: Proceedings of 17th International Conferenceon Crystal Growth and Epitaxy (ICCGE-17).

[38]M. Grundmann, T. Böntgen, and M. Lorenz, "Occurrence of rotation domains in heteroepitaxy," Phys. Rev. Lett. **105**, 146102 (2010).

[39]H. Peelaers, D. Steiauf, J. B. Varley, A. Janotti, and C. G. Van de Walle, "(In$_x$Ga$_{1-x}$)$_2$O$_3$ alloys for transparent electronics," Phys. Rev. B **92**, 085206 (2015).

[40]C. Kranert, J. Lenzner, M. Jenderka, M. Lorenz, H. von Wenckstern, R. Schmidt-Grund, and M. Grundmann, "Lattice parameters and Raman-active phonon modes of (In$_x$Ga$_{1-x}$)$_2$O$_3$ for $x < 0.4$," J. Appl. Phys. **116**, 013505 (2014).

[41]R. Hull and J. C. Bean, "Misfit dislocations in lattice-mismatched epitaxial films," Crit. Rev. Solid State Mater. Sci. **17**, 507 (1992).

21 March 2024 19:46:19